

Communication

Removing of Fe, Pb and Hg from Crude Selenium by Fractional Crystallization

Bei He ^{1,2,3}, Weiyi Wang ^{1,2,3}, Wenlong Jiang ^{1,2,3}, Baoqiang Xu ² and Hongwei Yang ^{1,2,3,*}

¹ Key Laboratory for Nonferrous Vacuum Metallurgy of Yunnan Province, Kunming University of Science and Technology, Kunming 650093, China

² National Engineering Research Center for Vacuum Metallurgy, Kunming University of Science and Technology, Kunming 650093, China

³ Faculty of Metallurgical and Energy Engineering, Kunming University of Science and Technology, Kunming 650093, China

* Correspondence: hongwei@kust.edu.cn; Tel.: +86-13-987-157-570

Abstract: This paper focuses on a fractional crystallization methodology using a rotating and internally gas-cooled crystallizer to purify crude selenium. Experiments using a rotating and gas-cooled crystallizer (cooled finger) were performed. The distribution coefficients of the main impurities (Pb, Fe and Hg) in selenium were presented as a polynomial function of concentration. The experimental parameters such as crystallization temperature and rotation rate were determined and discussed. The appropriate crystallization temperature is 222 °C and the rotation rates are 120 and 300 rpm, respectively. The purity of crude selenium increased from 99.9% to over 99.997%. Compared with the traditional method such as zone melting, this method only takes less than one day to complete several purifications, and the purification effect is better than the former. The removal rates of Hg, Pb and Fe in Se are 28.70%, 97.63% and 96.28%, respectively. The direct yield of Se purified is 92.5%. This study provides an efficient process for high-purity selenium, which has important industrial applications.

Keywords: fractional crystallization; selenium; purification



Citation: He, B.; Wang, W.; Jiang, W.; Xu, B.; Yang, H. Removing of Fe, Pb and Hg from Crude Selenium by Fractional Crystallization. *Metals* **2023**, *13*, 739. <https://doi.org/10.3390/met13040739>

Academic Editors: Norman Toro, Edelmira Gálvez and Ricardo Jeldres

Received: 13 March 2023

Revised: 29 March 2023

Accepted: 6 April 2023

Published: 10 April 2023



Copyright: © 2023 by the authors. Licensee MDPI, Basel, Switzerland. This article is an open access article distributed under the terms and conditions of the Creative Commons Attribution (CC BY) license (<https://creativecommons.org/licenses/by/4.0/>).

1. Introduction

Selenium is a nonmetallic, gray solid, one of the rare elements found in the earth's crust in small amounts. Berzelius, a Swedish chemist, discovered selenium in 1817; it has been widely used in various high-tech fields such as the electronics industry, photocells, solar cells, television and radio fax [1]. In addition, selenium can also be used in glass, pigment, metallurgy and other industries.

The superpurification of selenium is usually achieved by chemical and physical methods. Chemical purification includes hydrogenation reduction, selective leaching precipitation and thermal decomposition of hydrogen selenide [2–5]. These methods prepare intermediate compounds by adding chemical agents followed by impurity separation. The main physical methods are vacuum distillation and zone melting. Zha studied the process parameters such as saturated vapor pressure, actual evaporation rate and adjustment coefficient of selenium in vacuum distillation [6]. Zone melting involves the removal of impurities from crude selenium [7–9]. However, the process goes through many steps and takes several days to complete.

At present, more and more attention has been paid to researching the diverse uses of pollutant removal. The Awual group has produced some adsorptive materials to remove specific pollutants [10–12]. They directly fixed functional organic ligands onto mesoporous silica to prepare composite adsorbents for the detection and removal of toxic copper ions in contaminated water. They also studied the effect of chitosan-modified cotton cloth on removing reactive dyes from water. Awual et. al. fabricated optical composite materials for cadmium ion detection and removal from wastewater solutions. Irwing M. et. al. proposed

degrading emerging contaminants in water by the catalytic chemistry of micron-scale brass or copper-zinc alloy [13]. Wang et al. studied the Al–Ga–In–Sn alloy that can effectively remove p-CNB [14].

As an effective purification method, fractional crystallization has been widely used in the past decades. Curtolo studied the effect of process parameters on the purity of aluminum during rotary fractional crystallization [15,16]. Yaghy introduced the wax deposition rate and pseudo-steady-state deposition mass values [17]. Joshua explored the heat and mass transfer process of cold finger separation and pointed out that separation production was mainly affected by convection transfer controlled by cooling gas flow [18].

This paper focuses on the separation and purification of crude selenium by rotating internal air-cooled crystallizer. The rotational mechanism promotes homogeneous mixing of the melt and a stable boundary layer, ensuring optimal separation of impurities. The main impurities such as iron and lead in selenium were effectively removed by crystallization. Compared with other methods, the purification efficiency of this method is greatly improved.

2. Theory

The crystallization process of metals is complicated. On the one hand, solid phase precipitation from liquid phase will cause changes in material properties and structure. Crystallization, on the other hand, is accompanied by heat and mass transfer. The distribution coefficient K is generally defined as the ratio of the concentration of a component in the solid phase divided by the concentration in the liquid phase:

$$K = \frac{C_S}{C_L} \quad (1)$$

Values C_S and C_L are the concentrations of impurity in the solid phase and in the liquid phase, respectively.

The crystallization rate is not zero in the process of metal crystallizing. Therefore, the solid and liquid phases are not in equilibrium, and the purification effect should be expressed by the effective distribution coefficient (K_e). The effective distribution coefficient describes the ratio of the actual distribution of impurities in the solid-to-liquid phase, considering the influence of the kinetic process at the solid–liquid interface and the transport process near the liquid interface. The relationship between the distribution coefficient K and effective distribution coefficient K_e is as follows [19]:

$$K_e = \frac{K}{K + (1 - K)e^{-\frac{v\delta}{D}}} \quad (2)$$

According to Equation (2), the effective distribution coefficient K_e is related to distribution coefficient K , solidification velocity v , impurity enrichment layer thickness δ and diffusion coefficient D . When $\frac{v\delta}{D} = 0$, we have $K_e = K$; when $\frac{v\delta}{D} \rightarrow \infty$, then $K_e \rightarrow 1$. Therefore, the value of the effective distribution coefficient is between K and one. It means that the actual effect of crystallization on metal purification is lower than that of the equilibrium conditions, and it depends on whether the reaction is in equilibrium. This rule has important guiding significance for the process of metal crystallizing and refining. When $K_e = K$, the purification effect is the best. It is necessary to create conditions to reduce the thickness of the impurity enriched layer, so that the effective distribution coefficient is as close to the distribution coefficient as possible.

For a small enough growth rate, δ depends simply on the rotation rate and physical properties of the liquid phase [20].

$$\delta = 1.6D^{1/3}\nu^{1/6}\omega^{-1/2}, \quad (3)$$

where ν is the kinetic viscosity of the fluid and ω is the angular velocity of crystal rotation.

From Equation (3), δ will be reduced when increasing the angular velocity of “the cooled finger”. Furthermore, rotation leads to the reduction of the temperature gradient between the crystallization front and the melt beside the crucible wall, keeping the heat flow from the melt to the interface as small as possible. In a word, “the cooled finger” angular velocity ω has a great influence on the thickness of the impurity enrichment layer thickness δ . In order to explore the most suitable parameters such as cooled finger angular velocity for crystallization to remove impurities, crystallization experiments were carried out by a self-made rotating and gas-cooled crystallizer.

3. Experimental Procedure

A fractional crystallization device is used to study the impurity removal from selenium as shown in Figure 1. The structures include a vacuum system, temperature detection system, air cooling system, heating system and a crystallization pot. The height of the crystallizer is 148 cm, the outer diameter is 22 cm, and the inner diameter is 20 cm. The whole crystallizer can be divided into three sections, which are controlled by the hydraulic device to facilitate the operation of loading materials and replacing the crucible and other operations. The crucible used in the experiment is a cylindrical crucible with an inner diameter of 100 mm and an inner height of 225 mm. According to the different material densities, 2–10 kg of raw materials can be put into it at a time. The crude selenium comes from the product of laboratory distillation, and its composition is shown in Table 1. Standards 3N and 4N adopt the Chinese non-ferrous metal industry standard YS/T 1354-2020.

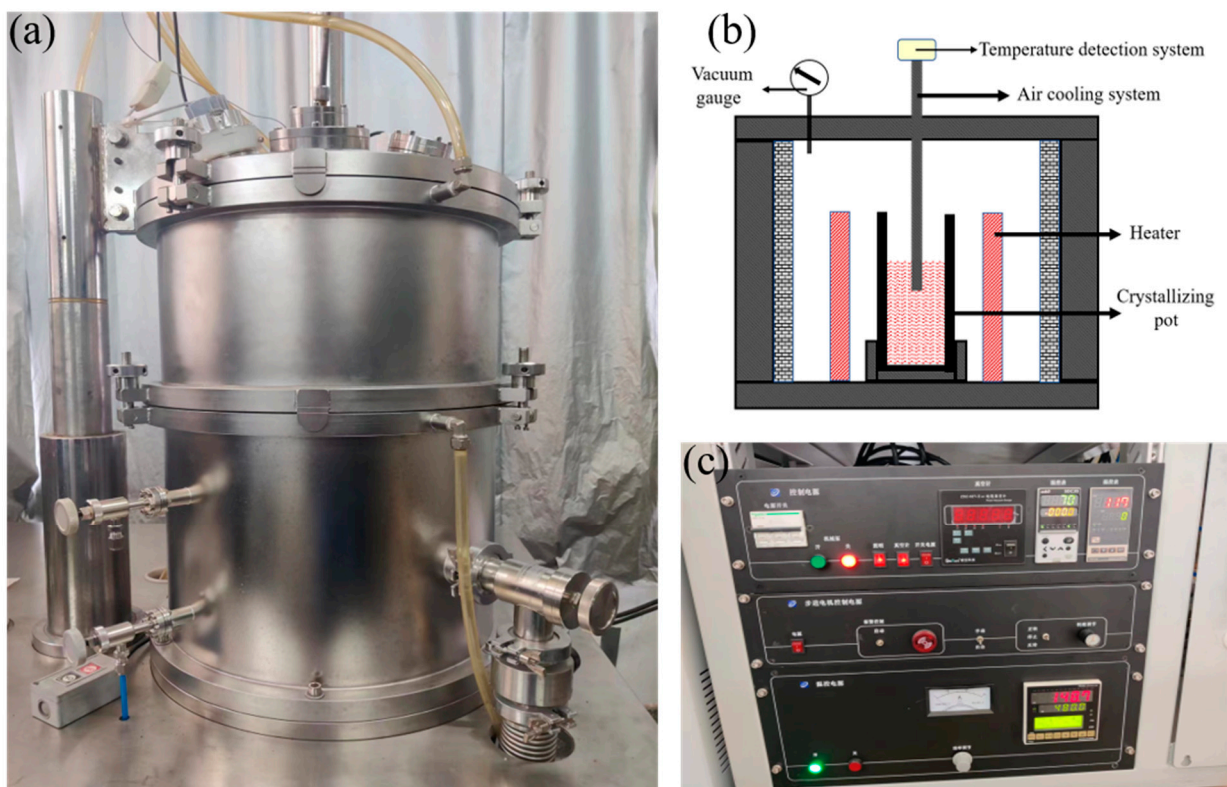


Figure 1. Diagram of rotating crystallizer: (a) photograph of the rotating crystallizer; (b) structural schematic diagram of the rotating crystallizer; (c) temperature control system of the rotating crystallizer.

Table 1. Raw material compositions (units: ppm).

| | Hg | Fe | Pb | As | Sb | Te | Bi | Al |
|----------------|-------|-------|-------|------|------|-------|------|------|
| Raw material 1 | 19.72 | 18.53 | 2.75 | 4.92 | 2.44 | 2.94 | 2.63 | 1.01 |
| Raw material 2 | 13.38 | 139 | 21.07 | 5.43 | 8.38 | 12.42 | 0.96 | 0.67 |
| 3N standard | 10 | 100 | 20 | 30 | 10 | 100 | / | / |
| 4N standard | 3 | 10 | 5 | 5 | 5 | 10 | 5 | 8 |

The crystallization process is shown in Figure 2. After putting crude selenium into the crucible, the equipment is vacuumed, and argon gas is pumped into the equipment. This process is repeated three times to ensure no oxidation occurs when the crude selenium is heated. A graphite heater is used to heat the samples and wrap around the crucible, and the temperature is controlled by an automatic temperature control system. During the holding time, the cooling gas flow rate is adjusted, and the temperature on the “cooled finger” is fine-tuned to ensure the stability of the temperature. At the beginning of the crystallization process, the temperature of the melt near the “cooled finger” decreases continuously through the blowing of gas in the “cooled finger” until the desired crystallization temperature is reached. The temperature is kept constant until the end of the experiment. The experimental scheme is designed to study the feasibility of the method, that is, to study the effects of crystallization temperature and rotation rates on crystallization. The enriched impurities are analyzed via inductively coupled plasma mass spectrometry (ICP-MS).

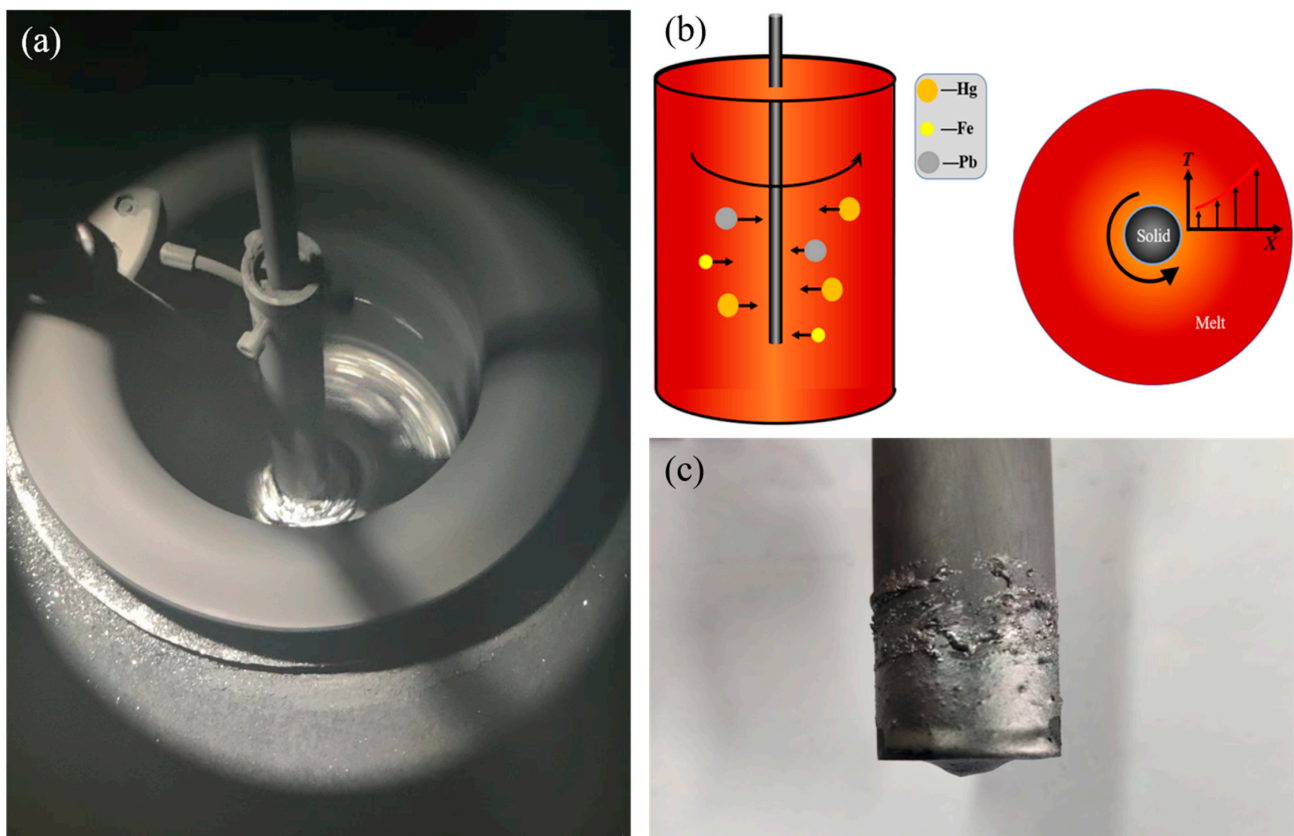


Figure 2. Schematic diagram of the principle of the crystallization process: (a) photograph of the crystallization process; (b) structural schematic diagram of the crystallization process; (c) the cooled finger.

4. Results and Discussion

4.1. Calculation of Distribution Coefficient

According to Equation (1), the distribution coefficient as a function of concentration was calculated based on the individual binary phase diagram of Se–X (X = Pb, Fe, Hg) systems [21]. Figure 3 shows the liquidus used for fitting. The X_S and X_L in the binary phase diagrams were defined as a polynomial function of concentration as $F = Ax^4 + Bx^3 + Cx^2 + Dx + E$. By substituting the temperature F into the fitting equation, x obtained by calculation is the concentration of impurity elements in selenium under the equilibrium state at a specific temperature, and this value is C_L in Equation (1). The abscissa of the closest solid phase line corresponding to C_L is the value of C_S . Divide C_S by C_L to obtain the distribution coefficient of impurities at a specific temperature. Table 2 shows the parameters of polynomial functions for each system.

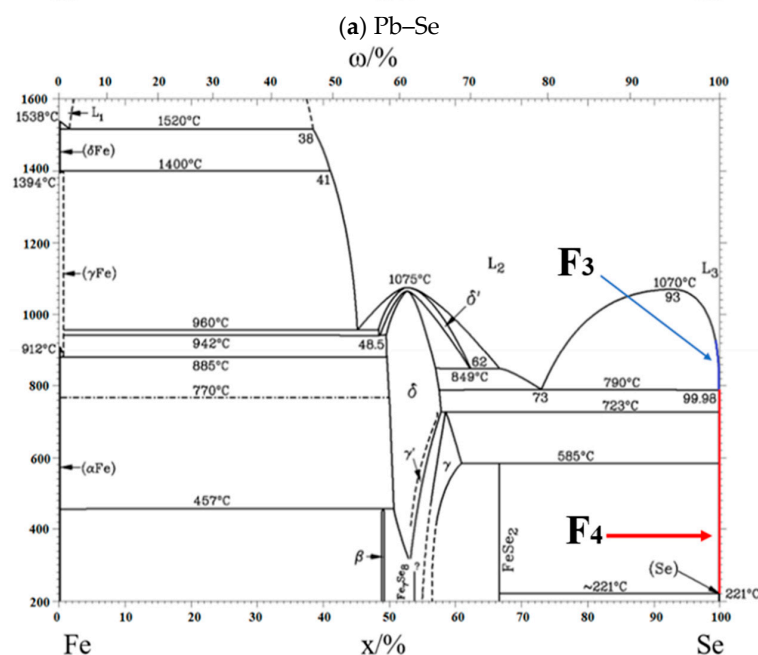
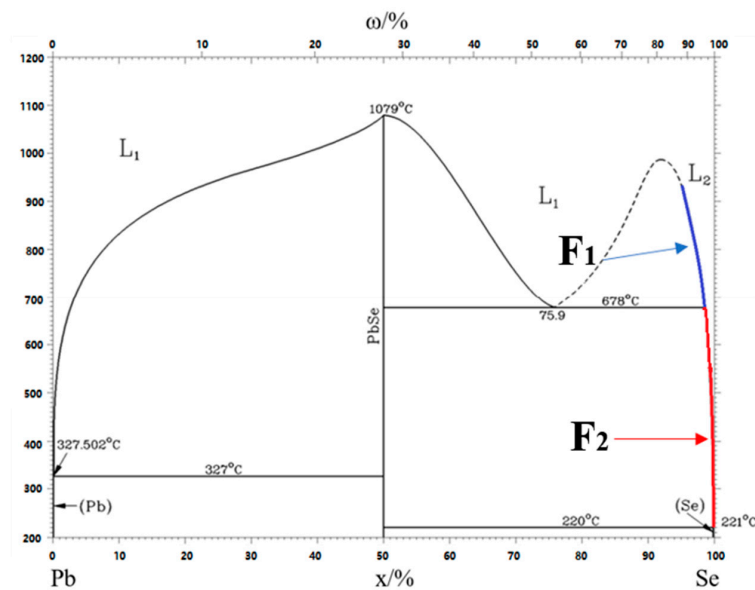


Figure 3. Cont.

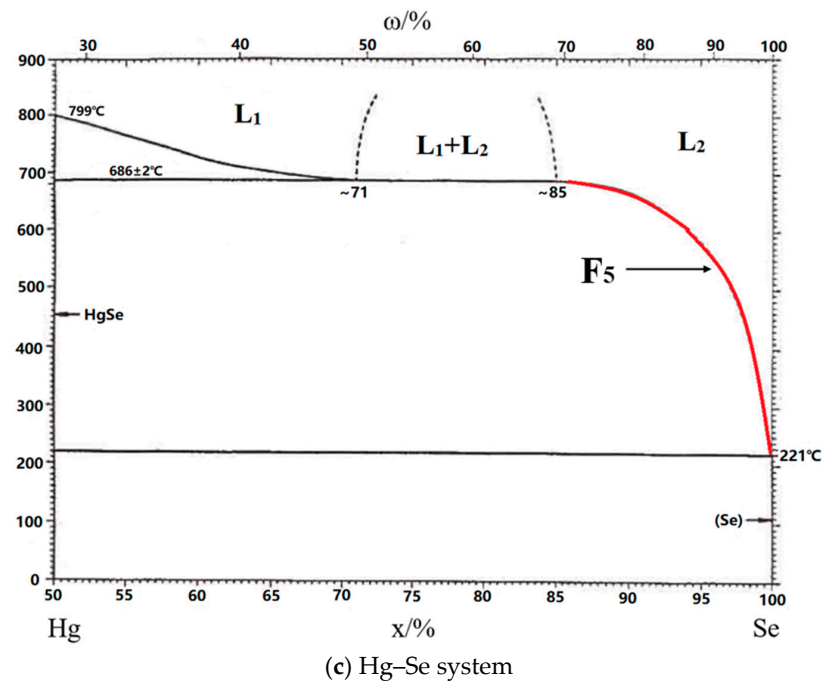


Figure 3. The liquidus curves used to fit: (a) Pb–Se system; (b) Fe–Se system and (c) Hg–Se system.

Table 2. The parameters of polynomial equations for Pb–Se, Fe–Se and Hg–Se systems.

| Equation | A | B | C | D | E | Range of x | R ² |
|------------------------|-------------------------|--------|--------|----------------------|------------------------|-------------|----------------|
| F ₁ (Pb–Se) | -6.681×10^{-4} | 0.1043 | 2.239 | 145.7 | 0 | 93.4–98.5% | 0.9986 |
| F ₂ (Pb–Se) | -2.357×10^{-2} | 4.646 | −228.9 | −6.271 | 840.2 | 98.5–100% | 0.9932 |
| F ₃ (Fe–Se) | −0.2769 | 55.27 | −2757 | −82.39 | −989.5 | 99.8–99.98% | 0.9995 |
| F ₄ (Fe–Se) | 0 | 0 | 0 | -2.845×10^4 | 2.845221×10^6 | 99.98–100% | 0.9989 |
| F ₅ (Hg–Se) | -3.496×10^{-3} | 0.9422 | −84.78 | 2554 | 0 | 86–100% | 0.9957 |

The coefficient of determination R^2 of the polynomial equation obtained is close to one and is highly reliable for calculating distribution coefficients. When the temperature is 222 °C, the distribution coefficients of the main impurities Pb, Fe and Hg in selenium are 10.36, 16.07 and 6.25, respectively. For the system with $K > 1$, the impurities are enriched in the solid phase during crystallization. The larger the deviation between K and one, the better the crystallization effect.

4.2. Crystallization Temperature

Experiments at different crystallization temperatures are carried out, and the results are shown in Table 3. It can be seen from Table 3 that 222 °C is the most suitable temperature for impurity enrichment and crystallization. Since the melting point of selenium is 222 °C, if the melt temperature is lower than 222 °C, there will be a large amount of selenium melt attached to the “cooled finger” and the effect of removing impurities is not obvious. When the temperature is higher than 222 °C, the impurities enriched by crystallization will melt with the increase of temperature, which makes it difficult to enrich.

Table 3. The compositions of crystallization products at different temperatures.

| Temperature/°C | Rotation Speed/rpm | Holding Time/min | Hg/ppm | Pb/ppm | Fe/ppm |
|----------------|--------------------|------------------|--------|--------|--------|
| 212 | 120 | 120 | 7.84 | 23.31 | 254 |
| 217 | 120 | 120 | 9.52 | 15.35 | 387 |
| 222 | 120 | 120 | 27.03 | 18.43 | 899 |
| 227 | 120 | 120 | 15.51 | 11.71 | 512 |
| 232 | 120 | 120 | 12.46 | 13.37 | 311 |
| Raw material 1 | | | 19.72 | 2.75 | 18.53 |

4.3. Rotation Rate

The crude selenium in the crucible was kept at 230 °C to study whether the density affects the separation of impurities, as shown in Figure 4. A total of 73.37 g of raw material was put into a crucible, and the weight was 73.36 g at the end of the experiment, only 0.01 g of crude selenium was volatilized. The specific compositions of solid phase are listed in Table 4. Impurities are Pb, Fe, Hg and other elements.

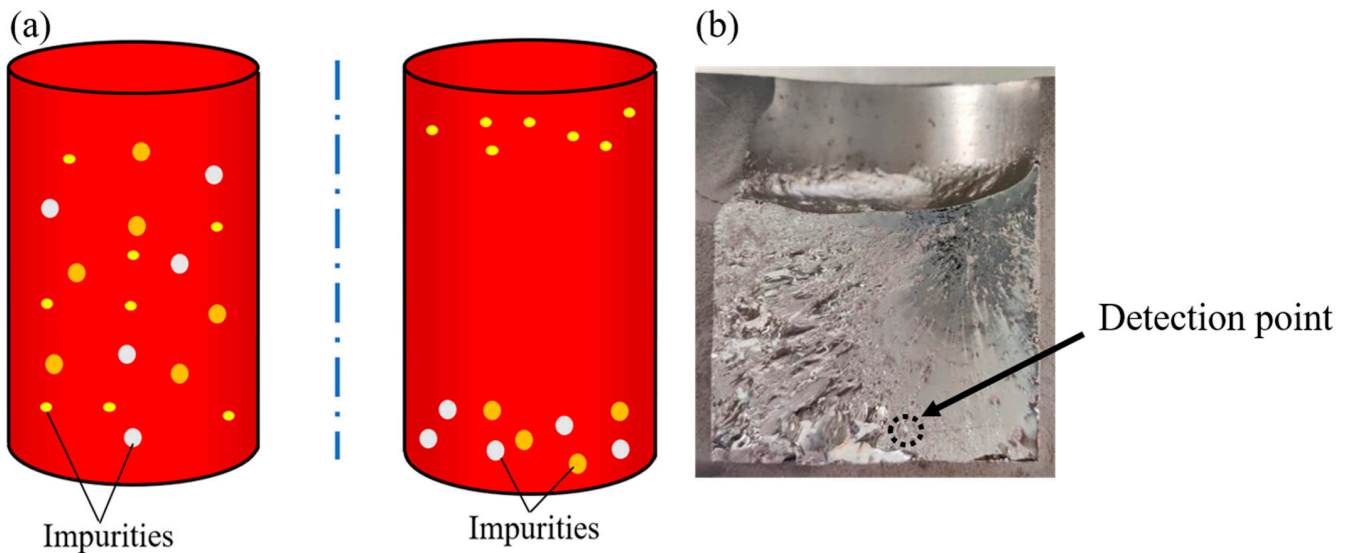


Figure 4. Diagram of the effect of density on impurity separation: (a) diagram of the static experiment; (b) photograph of the static experiment.

Table 4. Sample compositions of static experiment (units: ppm).

| | Hg | Fe | Pb | As | Sb | Te | Bi | Al |
|----------------|-------|-------|------|------|------|------|------|------|
| Sample | 19.44 | 18.53 | 3.52 | 5.76 | 8.49 | 7.03 | 0.31 | 4.22 |
| Raw material 1 | 19.72 | 18.53 | 2.75 | 4.93 | 2.44 | 2.94 | 2.63 | 1.01 |
| 3N standard | 10 | 100 | 20 | 30 | 10 | 100 | / | / |

We found that melting and static sedimentation had poor effect on the separation of selenium impurities and needed to change the experimental conditions to remove the impurities.

Five rotation rates were selected to determine the most suitable parameter. The effect of crystallization rotation rate on impurity enrichment was investigated, and the optimum crystallization rotation rates were obtained. The enriched impurities were analyzed by ICP-MS, and the enrichment factors were compared. The enrichment factor is defined as the ratio of concentration on the “cooled finger” to the initial one, subtracted from 100%, which is

$$\text{Enrichment Factor} = \left(\frac{C_S}{C_0} - 1 \right) \times 100\% \quad (4)$$

The greater the enrichment factor, the more metallic impurities are removed. Enrichment factors of Pb, Fe and Hg, the main impurities in selenium, are shown in Figure 5. It reveals that the enrichment factor of each impurity varies significantly under different rotation rates. At 120 rounds per minute (rpm), the enrichment factor of Hg is the largest, and at 300 rpm, the enrichment factor of Pb is the largest. The enrichment factor of Fe is positive in the whole range and is suitable for removal by fractional crystallization.

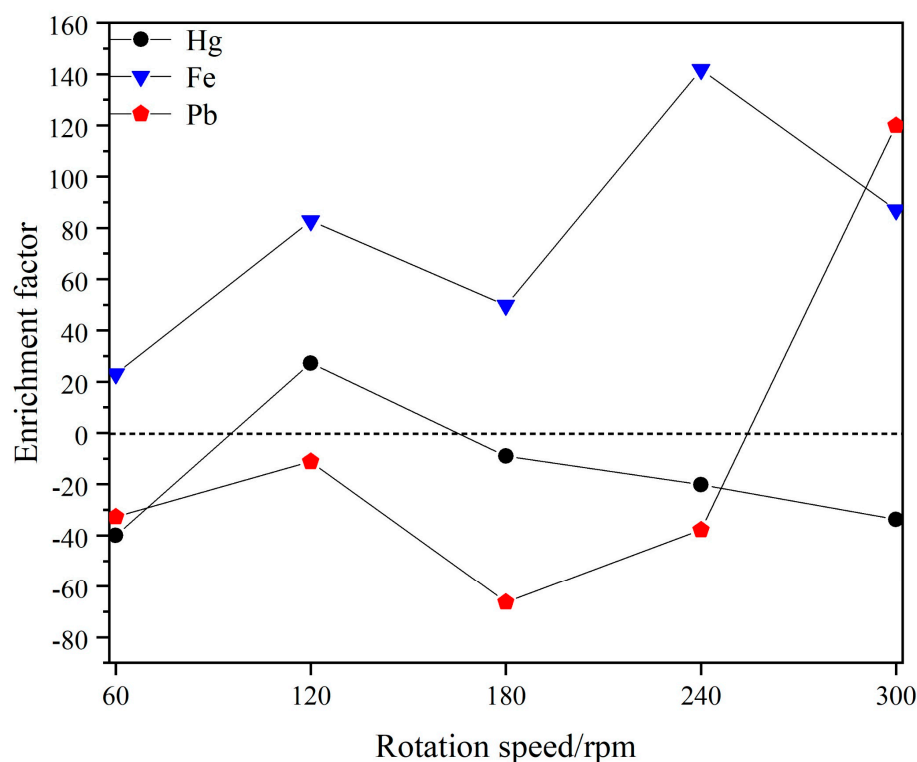


Figure 5. Enrichment factors of main impurities in selenium at different rotational rates.

4.4. Purification of Crude Selenium

From Table 3 and Figure 5, it is found that 222 °C and 120 rpm are the most conducive parameters for Hg removal. The best conditions for removing Pb are 222 °C and 300 rpm. At the same time, Fe is easily removed in the whole range.

After nine passes of crystallization, the impurity contents in crude Se are shown in Table 5. The volatile substances produced in the crystallization process were analyzed, and the contents of Hg, Pb and Fe are 437, 560 and 68.07 ppm, respectively.

Table 5. The impurity content in crude selenium after different crystallization times.

| Crystallization Times | Mass/g | Impurity Content/ppm | | | |
|-----------------------|--------|----------------------|-------|-------|------|
| | | Pb | Fe | Hg | As |
| Raw material 2 | 2000 | 21.07 | 139 | 13.38 | 5.43 |
| 1 | 1986 | 18.71 | 95 | 12.45 | 5.10 |
| 3 | 1947 | 10.27 | 33.81 | 10.25 | 4.66 |
| 5 | 1914 | 5.63 | 16.19 | 9.86 | 4.21 |
| 7 | 1887 | 2.48 | 11.83 | 9.72 | 3.86 |
| 9 | 1853 | <0.5 | 5.17 | 9.54 | 3.15 |
| Crystallization Times | Mass/g | Sb | Te | Bi | Al |
| Raw material 2 | 2000 | 8.38 | 12.42 | 0.96 | 0.67 |
| 1 | 1981 | 7.13 | 10.57 | 0.61 | <0.5 |
| 3 | 1943 | 5.45 | 6.31 | <0.5 | <0.5 |
| 5 | 1903 | 3.84 | 4.55 | <0.5 | <0.5 |
| 7 | 1884 | 3.41 | 3.78 | <0.5 | <0.5 |
| 9 | 1853 | 2.89 | 2.27 | <0.5 | <0.5 |

The removal rates of the main impurities Hg, Pb and Fe in Se are 28.70%, 97.63% and 96.28%, respectively. The direct yield of Se purified to 99.997% is 92.5%, and the result is satisfactory.

5. Conclusions

Fractional crystallization separation experiments of crude selenium under different conditions were investigated. The results are in agreement with the theoretical calculation of fractional crystallization. The relationship between impurity concentration in crude selenium and crystallization temperature and rotation rate was discussed.

The selenium-rich liquidus curves of the Pb–Se, Fe–Se and Hg–Se systems were fitted to polynomial equations. The distribution coefficients of main impurities Pb, Fe and Hg in selenium are 10.36, 16.07 and 6.25, respectively. These values are greater than one, so impurities are enriched in the solid phase. The experimental results show that the optimum crystallization temperature of fractional crystallization is 222 °C. The rotational speed of 120 rpm is the best for mercury enrichment. The rotational speed of 300 rpm is the best condition for removing lead impurities. The enrichment performance of iron is better at different rotational speeds. The impurity in selenium can be effectively removed by fractional crystallization.

Author Contributions: Formal analysis, W.W.; resources, W.J.; writing—original draft preparation, B.H.; writing—review and editing, H.Y.; data analysis, W.J. and B.X.; funding acquisition, B.X. All authors have read and agreed to the published version of the manuscript.

Funding: This research was funded by the Fund of National Natural Science Foundation of China under Grant No. U1902221 and National Key R&D Program under Grant No. 2022YFC2904900. The APC was funded by the Fund of National Natural Science Foundation of China under Grant No. U1902221.

Data Availability Statement: The data that support the findings of this study are available from the corresponding author upon reasonable request.

Conflicts of Interest: The authors declare no conflict of interest.

References

1. Boyd, R. Selenium stories. *Nat. Chem.* **2011**, *3*, 570. [[CrossRef](#)] [[PubMed](#)]
2. Gustafsson, A.M.K.; Foreman, M.R.S.J.; Ekberg, C. Recycling of high purity selenium from CIGS solar cell waste materials. *Waste Manag.* **2014**, *34*, 1775–1782. [[CrossRef](#)] [[PubMed](#)]
3. Jiafeng, Z.; Bao, Z.; Xueyi, G.; Danqing, Z.; Chao, S.; Qian, L. Study on crude selenium purifying by a sulfite sodium leaching method. *Rare Met. Mater. Eng.* **2011**, *40*, 121–125. (In Chinese)
4. Pearson, R.K.; Haugen, G.R. Kinetics of the thermal decomposition of H₂Se. *Int. J. Hydrog. Energy* **1981**, *6*, 509–519. [[CrossRef](#)]
5. Nielsen, S.; Heritage, R.J. A method for the purification of selenium. *J. Electrochem. Soc.* **1959**, *106*, 39. [[CrossRef](#)]
6. Zha, G.; Wang, Y.; Cheng, M.; Huang, D.; Jiang, W.; Xu, B.; Yang, B. Purification of crude selenium by vacuum distillation and analysis. *J. Mater. Res. Technol.* **2020**, *9*, 2926–2933. [[CrossRef](#)]
7. Burger, A.; Henderson, D.O.; Morgan, S.H.; Feng, J.; Silberman, E. Purification of selenium by zone refining. *J. Cryst. Growth* **1990**, *106*, 34–37. [[CrossRef](#)]
8. Feldewerth, G.B.; Bollong, A.B.I.; Bunnell, D.C. Preparation of High Purity Elements. U.S. Patent 5,513,834, 7 May 1996.
9. Su, C.H.; Sha, Y.G. Segregation coefficients of impurities in selenium by zone refining. *J. Cryst. Growth* **1998**, *187*, 569–572. [[CrossRef](#)]
10. Salman, S.; Hasan, N.; Hasan, M.; Kubra, K.T.; Sheikh, C.; Rehan, A.I.; Waliullah, R.; Rasee, A.I.; Awual, E.; Hossain, M.S.; et al. Improving copper (II) ion detection and adsorption from wastewater by the ligand-functionalized composite adsorbent. *J. Mol. Struct.* **2023**, *1282*, 135259. [[CrossRef](#)]
11. Salman, S.; Sheikh, C.; Hasan, M.; Hasan, N.; Kubra, K.T.; Rehan, A.I.; Awual, E.; Rasee, A.I.; Waliullah, R.; Hossain, M.S.; et al. Chitosan-coated cotton fiber composite for efficient toxic dye encapsulation from aqueous media. *Appl. Surf. Sci.* **2023**, *622*, 157008. [[CrossRef](#)]
12. Hasan, M.; Kubra, K.T.; Hasan, N.; Awual, E.; Salman, S.; Sheikh, C.; Rehan, A.I.; Rasee, A.I.; Waliullah, R.; Islam, S.; et al. Sustainable ligand-modified based composite material for the selective and effective cadmium (II) capturing from wastewater. *J. Mol. Liq.* **2023**, *371*, 121125. [[CrossRef](#)]
13. Ramirez-Sanchez, I.M.; Apul, O.G.; Saleh, N.B. Photocatalytic activity of micron-scale brass on emerging pollutant degradation in water: Mechanism elucidation and removal efficacy assessment. *RSC Adv.* **2020**, *10*, 39931–39942. [[CrossRef](#)] [[PubMed](#)]
14. Wang, Q.; Chen, J.; Zhao, J.; Cao, Y.; Li, J.; Liu, H.; Chen, F. Removal of p-chloronitrobenzene from wastewater by aluminum and low melting point metals (Al-Ga-In-Sn) alloy. *J. Environ. Chem. Eng.* **2021**, *9*, 106339. [[CrossRef](#)]
15. Friedrich, S.; Curtolo, D.C.; Friedrich, B. Effect of process parameter variation on purity during rotary fractional crystallization of Aluminum. *Open J. Met.* **2017**, *7*, 25. [[CrossRef](#)]

16. Curtolo, D.C.; Friedrich, S.; Bellin, D.; Nayak, G.S.; Friedrich, B. Definition of a first process window for purification of aluminum via “Cooled Finger” crystallization technique. *Metals* **2017**, *7*, 341. [[CrossRef](#)]
17. Yaghy, G.; Ali, A.; Charpentier, T.V.J.; Fusi, L.; Neville, A.; Harbottle, D. Wax deposition using a cold rotating finger: An empirical and theoretical assessment in thermally driven and sloughing regimes. *J. Pet. Sci. Eng.* **2021**, *200*, 108252. [[CrossRef](#)]
18. Versey, J.R.; Phongikaroon, S.; Simpson, M.F. Separation of CsCl from LiCl-CsCl molten salt by cold finger melt crystallization. *Nucl. Eng. Technol.* **2014**, *46*, 395–406. [[CrossRef](#)]
19. Qiu, K.; Chen, Q. Thermodynamical principle of metal refining by fractional crystallization from metals. *Nonferrous Met.* **1999**, *51*, 43–48. (In Chinese)
20. Burton, J.A.; Prim, R.C.; Slichter, W.P. The distribution of solute in crystals grown from the melt. Part I. Theoretical. *J. Chem. Phys.* **1953**, *21*, 1987–1991. [[CrossRef](#)]
21. Thaddeus, B.; Massalski, T.B. *Binary Phase Diagrams*, 2nd ed.; Plus Updates; ASM International, The Materials Information Society: Russell Township, OH, USA, 1996.

Disclaimer/Publisher’s Note: The statements, opinions and data contained in all publications are solely those of the individual author(s) and contributor(s) and not of MDPI and/or the editor(s). MDPI and/or the editor(s) disclaim responsibility for any injury to people or property resulting from any ideas, methods, instructions or products referred to in the content.